Generalized Anisotropic Planar Rotor Model and Its Application to Polymer Intercalation Compounds

Guomin Mao,[1,*] Dong Chen,[1,†] F. E. Karasz,[2] and M. J. Winokur[1]

[1]*Department of Physics, University of Wisconsin, Madison, Wisconsin 53706*
[2]*Department of Polymer Science and Engineering, University of Massachusetts, Amherst, Massachusetts 01003*

A diverse structural phase progression is observed in diffraction studies of an alkali-metal intercalated conducting polymer, poly(*p*-phenylene vinylene), as functions of both temperature and chemical potential. Despite the presence of translational displacements, extensive disorder, and other experimental host limitations, an equivalent heuristic structural counterpart appears in a phase diagram derived using a modified anisotropic planar rotor Hamiltonian (introduced and studied by Choi, Harris, and Mele). This model includes only rotational motions and therefore demonstrates that much of the underlying structural evolution is governed by only a few key degrees of freedom.

Intercalation is a widespread process marked by a complex interplay between competing molecular-level interactions and, subsequently, the appearance of striking structural phases and unusual phase behavior [1]. Formation of intercalation compounds is often encountered in highly anisotropic host systems ranging from the quasi-two-dimensional layered materials (e.g., graphites or silicates) down to "zero" dimensional forms (e.g., C_{60}). Intermediate to these are the quasi-one-dimensional hosts, primarily π-conjugated polymers, characterized by strong covalent bonding along the chain axis and weaker inter-chain interactions in the orthogonal directions. Polymer intercalation is especially diverse because it often elicits both rotational and translational responses by the host chains [2].

Elucidating both the underlying mechanisms by which these guest-host compounds are formed and the key molecular-level degrees of freedom involved has proven difficult. The overall complexity of the chain structure in tandem with extensive and systemic disorder limits the use of a first-principles approach. Alternatively, this problem can be cast in a phenomenological setting by postulating and parametrizing the most important guest-host interactions. In particular, an extension of the generalized anisotropic planar rotor model [3] to include guest-host interactions [by Choi, Harris, and Mele (CHM) [4,5]] has been successful in justifying experimental claims for a novel phase behavior [6] and has facilitated identification of certain low-symmetry structures [7]. Still, the CHM model itself exhibits an exceptionally rich range of phase behavior as a function of temperature T, chemical potential μ, and the relative interaction parameter strengths [5] whose overall applicability has, at best, remained tentative.

This Letter demonstrates that the CHM model, despite its functional simplicity, effectively describes the underlying structural behavior within conjugated polymer systems dominated by chain rotations, specifically alkali-metal intercalated poly(*p*-phenylene vinylene) (PPV), as a function of *both* T and μ. With respect to variations of μ, both mean-field theory studies [5] and recent Monte Carlo simulations [8] have identified numerous stoichiometric structural phases, some of which reach exceedingly high alkali-metal concentrations. Experimental confirmation of these structures is, as yet, undocumented. A second defining CHM model attribute is a predicted, but hitherto unidentified, low-temperature instability in the well-known high-symmetry 120° phase [6,9,10]. Employing the results of the CHM model as a heuristic guide, we identify these attributes and decipher the *full* set of equatorial (i.e., perpendicular to the PPV chain axis) scattering data even though these materials have properties [2] that lie outside the implicit CHM model constraints.

The stated form of the CHM model Hamiltonian includes only terms arising from low-order polymer mass distribution moments rigidly anchored onto a triangular lattice. The basic interaction between planar rotors [3], H_0, appears as

$$H_0 = \alpha \sum_{\langle i,j \rangle} \cos(2\theta_i - 2\theta_j)$$
$$+ \beta \sum_{\langle i,j \rangle} \cos(2\theta_i - 2\phi_{ij})\cos(2\theta_j - 2\phi_{ij}), \quad (1)$$

where the summations extend over only nearest neighbors, α and β are arbitrary interaction parameters, θ_i and θ_j represent the angular orientation of adjacent rotors, and the angle ϕ_{ij} is determined by the symmetry of the underlying lattice (see Fig. 1 inset). These two terms respectively represent the isotropic and anisotropic portions of the interaction potential and establish a competition that, at low T, can lead to a herringbone-sine (HBs) (shown in Fig. 1) packing motif often observed in conducting polymers such as polyacetylene and PPV. The CHM postulated pairwise interaction between the three nearest planar rotors and a typical intercalant channel site is represented by

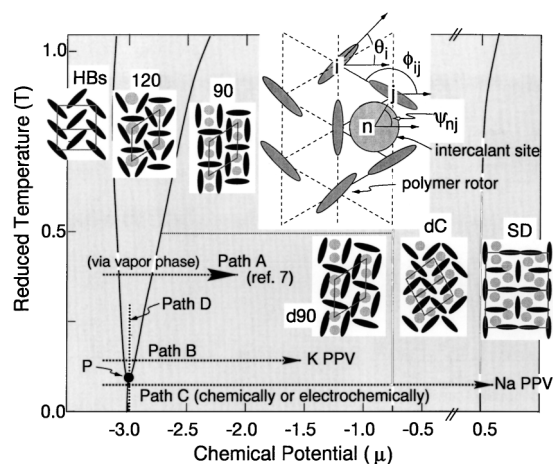$$H_{int} = \gamma \sum_{n,k} \cos(2\theta_k - 2\psi_{nk}), \quad (2)$$

FIG. 1. CHM model (see text) phase diagram reported in Ref. [5] for model parameters α, β, and γ of -1, 2, and 3, respectively, in conjunction with various pathway addressed by this work and schematic drawings of the various stoichiometric phases [HBs, herringbone-sine; 120 ($n = 1/3$), 120° phase; 90, 90° phase; $d90$ ($n = 2/3$), distorted 90°; dC ($n = 1$), distorted herringbone cosine; SD ($n = 4/3$), serpentine dense]. Inset: schematic of the CHM model construction.

where ψ_{nk} is the given angle of the vector connecting the kth rotor and the nth channel site. Positive values of the interaction parameter γ tend to orient the major axis of the rotors, surrounding a filled site, perpendicular to the vector connecting this site to a point specified by each rotor mass center.

The total Hamiltonian is thus $H = H_0 + H_{int}$. Temperature and other parameters appear here in reduced form with respect to $|\alpha|$. With the exception of the ratio $\beta/|\alpha| \approx 2$ (appropriate for quadrupole pair interactions), current theory and experiment place few constraints on γ although γ *will* be intercalant specie (or size) specific. At nominal α, β, and γ values of -1, 2, and 3, respectively, the low-temperature region of the μ-T phase diagram (reproduced in Fig. 1) of Harris [5] exhibits four distinct two-dimensional (2D) packing motifs with stoichiometric alkali-metal channel/planar rotor occupancies, defined as n, of 1/3, 2/3, 1, and 4/3. The out-of-plane alkali-metal spacing along a channel is not specified by the CHM model but, experimentally, these typically range between 4 and 6 Å. This is used to specify a bulk alkali-metal concentration/PPV chain repeat as x (i.e., as alkali$_x$PPV with PPV $\equiv C_6H_4$). With respect to alkali-metal intercalated PPV samples, prepared by exposure to alkali-metal vapor at elevated temperatures, recent accounts [7] have identified the HBs $\rightarrow$ 120° $\rightarrow$ $d90$° transformation (path A in Fig. 1). Experimentally, these cited $d90$° phases do not reflect a perfect mapping to theory because there are translational distortions which effectively lower the unit cell symmetry (and broaden the scattering peaks). For the CHM model calculations this phase sequence extends over a large range of reduced γ values. A striking aspect within the CHM picture is that, for γ's un-

der 4, the 120° phase becomes thermodynamically unstable at low T leading to either a direct HBs $\rightarrow$ $d90$° phase transformation with respect to increasing μ (from paths A or B to C) or a 120° $\rightarrow$ HBs $+$ $d90$° phase separation with reduced temperature at point P along path D.

The present results are from uniaxially oriented, thin multilayer films (5–20 μm each) of PPV intercalated via vapor-phase [9], chemical [11], and/or electrochemical methods [12] in combination with *in situ* or *ex situ* "doping" cells. The chemical cells used Na or K/napthalene complexes dissolved in tetrahydrofuran (THF) while the electrochemical cell employed a sodium tetraphenylborate/THF electrolyte. Electrochemical intercalation complements the chemical method by allowing for an independent measurement of the alkali-metal concentration and better compositional control. The actual PPV unit cell [13,14] is monoclinic but, for the discussion that follows, the PPV chains are treated as extended planar rotors whose mass centers approximate a triangular lattice (of $a \approx 5$ Å). X-ray measurements were performed on either of two diffractometers using monochromatic Cu K_α (1.542 Å) radiation and, when necessary, a conventional cryostat. In the following account only equatorial ($hk0$) scattering data is shown although nonequatorial data was also recorded. The equatorial profiles represent scattering by the 2D lateral packing of the alkali-metal and polymer chains. The relatively high PPV film crystallinity ($\geq$90%) and slow doping kinetics [15] dictated long cycle times. These ranged from a few days (in the vapor-phase cells) to a few months (chemical cells) to nearly 18 months (electrochemical cells). In almost all cases the representative experimental profiles are compared to the prospective model structures using structure factor calculations (a customized Rietvelt refinement package [16]).

Nearly pure 120° phase K$_{0.5}$PPV and Na$_{0.5}$PPV samples, prepared by vapor-phase intercalation, were studied at room [9] and reduced temperatures [16] and representative profiles are shown in Fig. 2, respectively, on the left and right. In retrospect these data manifest clear features which establish the existence of a *reversible* low-temperature phase transition cited along path D (in Fig. 1). For the K$_{0.5}$PPV sample the most obvious of these are the two new reflections identified as the HBs (210) and $d90$ (200), and a reversible change in the 120° "(100)" intensity on thermal cycling. Modeling of the data by simply assuming changes in the 120° phase gave poor results. Excellent fits were obtained using a superposition of the original 120° phase, monotonically decreasing (on cooling), while comparable fractions [17] of the HBs and the $d90$° phases increase. The kinetics are very slow so that the scattering pattern evolves over extended "annealing" times. Analogous changes occur in the Na$_{0.5}$PPV 120° phase sample at room temperature and it too transforms, albeit very slowly, to a combination of HBs and $d90$° phases. Accounting for the temperature
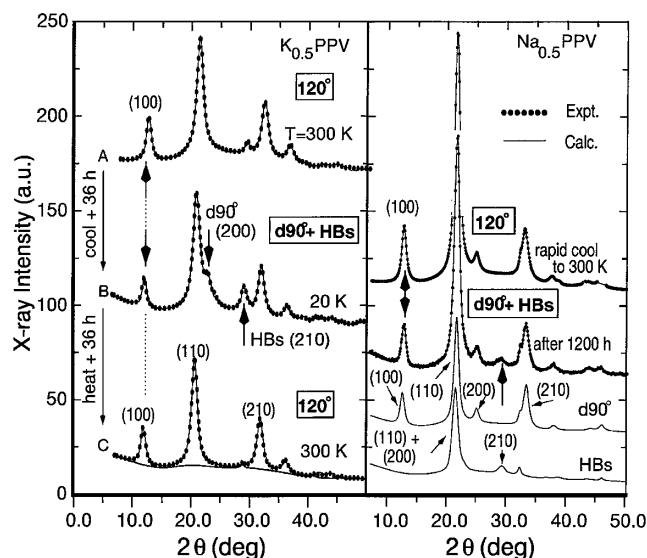
FIG. 2. Selected equatorial ($hk0$) data (black dots) in combination with calculated profiles (thin solid lines) from vapor intercalated K_xPPV (left panel) and Na_xPPV (right panel) initially in the 120° phase (at top) demonstrating the transformation to a two phase mixture of the HBs and $d90°$ phases (along path D in Fig. 1). Bold arrows highlight the key experimental features (see text) associated with this transition. The two bottom curves in the right panel are the individual calculated HBs and $d90°$ profiles used to fit the $d90°$ + HBs data. Note, for clarity all curves have been offset and the K_xPPV data proportionately rescaled.
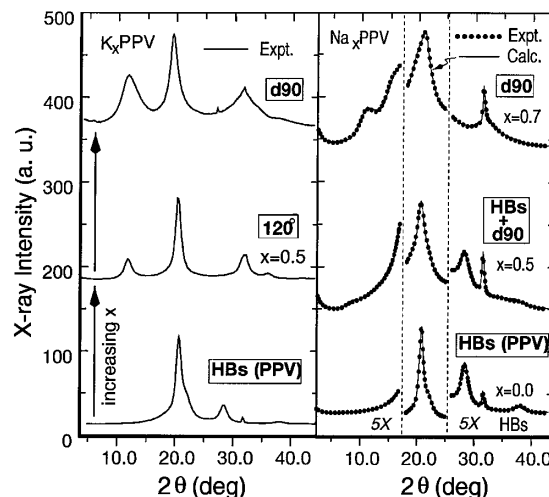

FIG. 3. Selected equatorial data in combination with calculated profiles (on right only) from chemically intercalated K_xPPV (along path B in Fig. 1) and electrochemically intercalated Na_xPPV (along path C) films. Note that all but the bottom two curves have been offset and scaled for clarity. A sharp feature near $2\theta = 32°$ arises from NaCl residues.

difference is easily accomplished by noting that, while a reduced $\gamma \approx 3$ is nominally correct, in reality $\gamma_K > \gamma_{Na}$, thus altering the relative position of point P in Fig. 1 with respect to horizontal and vertical pathways.

Without the guidance of the phase diagram in Fig. 1 this transition is difficult to unambiguously characterize. One complication arises from the subtle intensity differences between the 120° and $d90°$ phases. Unlike the $120° \rightarrow d90°$ transformation along path A during continued alkali-metal uptake, this thermal transition occurs at fixed composition x and does not elicit translational distortions of the underlying lattice. Only chain rotations and alkali-metal site occupancy variations occur and these merely alter the Bragg intensities while simultaneously being superimposed on the residual 120° phase signal. Since these polymers exist as extended chain rotors, a second constraint involves the extensive migration of the alkali-metal ions, almost certainly parallel to the PPV chain axis, which is necessary to form a heterogeneous mixture of the HBs ($x \ll 0.5$), the $d90°$ phase ($x \gg 0.5$), and the original 120° ($x \approx 0.5$) structure. These HBs structures are unlikely to revert to pure undoped PPV (at $x = 0.0$).

To further demonstrate the applicability of the CHM model phase diagram, Fig. 3 displays new data recorded at room temperature during chemical (paths B and C) or electrochemical intercalation (path C), thus probing the structure while effectively sweeping the chemical

potential (μ). Intercalation of the Na_xPPV sample (along path C) always occurs without a 120° phase formation. All data, up to intermediate alkali-metal compositions, can be suitably modeled only by a superposition of the HBs and a low-symmetry $d90°$ phase [7]. In contrast, the K_xPPV sample (following path B) evolves from pure PPV (HBs) through a coexistence of HBs and 120° to nearly pure 120° phase and then a gradual reduction of the 120° phase in combination with increasing contributions by the $d90°$ phase as in vapor-phase intercalation [7] (path A). These two distinct outcomes reconfirm the claim that only the 120° phase of K_xPPV is thermodynamically stable at room temperature.

As a final test of this CHM model phase diagram for establishing PPV structural evolution even at higher alkali-metal compositions (or large μ), Fig. 4 displays recent data from Na_xPPV samples at large x (the rightmost portions of path C in Fig. 1). For both intercalation methods the relatively broad features of the $d90°$ scattering profiles are replaced by noticeably sharper scattering features indicative of a new structural phase. This phase itself, at the highest alkali-metal concentrations, is superseded by a *second* new phase with very broad peak line shapes. This latter structure is especially unusual because of the appearance of a peak at lower 2θ and indicates a large unit cell repeat.

The CHM model phase diagram provides crucial guidance by identifying two distinct structural motifs at large μ (dC and SD in Fig. 1). The first has been considered in mean-field studies by Harris [5] and is referred to as a distorted herringbone-cosine phase (dC with $n = 1$). Larger unit cell structures were not generally considered by [5]. Extending our recent Monte Carlo studies [8]
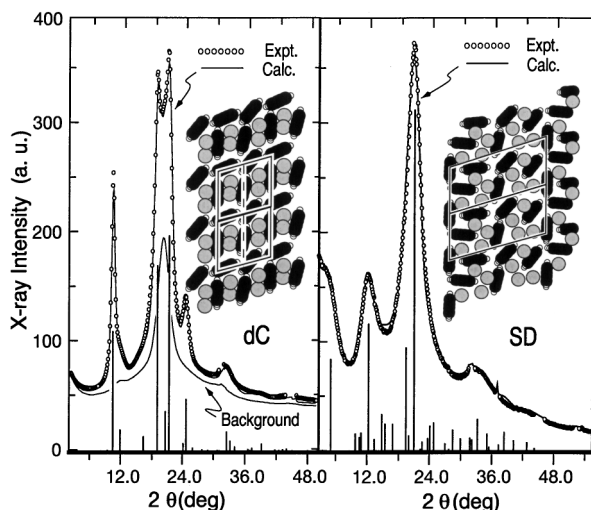
FIG. 4. Selected equatorial data and calculated profiles from electrochemically intercalated (on left) and chemically intercalated [18] (on right) $Na_x PPV$ in the dC and SD phases of Fig. 1. The insets depict the actual dC and SD model unit cells. Both frames also display, as vertical bars, the underlying Bragg peaks.

of the CHM Hamiltonian up to an $n = 4/3$ and α, β and γ values of -1, 2, and 3, respectively, yields a new, large-period ground-state structure whose meandering formations of the intercalant are designated as the "serpentine-dense" (SD) phase. Figure 4 displays direct comparisons of the $Na_{1.0}PPV$ electrochemical data (dC, at left) and a chemical intercalation data set (SD, at right) with curves from calculated model refinements. Both calculated profiles clearly demonstrate that each of these high-density intercalation phases has merit when used to assess the 2D packing within these new structural forms. The experimental dC unit cell size ($a = 9.6$ Å, $b = 17.2$ Å, and $\gamma = 107°$) is actually twice that of the CHM picture and both (SD, $a = 18.9$ Å, $b = 8.5$ Å, and $\gamma = 108°$) are oblique. Thus, as is generally true for most polymer intercalation structures, the experimental dC and SD phases include displacements which result in lower symmetry structures.

In summary we have demonstrated that a diverse set of alkali-metal intercalated PPV scattering data follows a phase diagram derived from a very simplified theoretical construct. From this we conclude that the CHM model embodies the essential guest-host interactions for speci-

fying the underlying structural evolution in this family of polymeric hosts. This success may also indicate that structural complexity seen elsewhere in polymer intercalation compounds may be similarly addressed and clarified.

*Current address: ANL, Argonne, IL 60439.
†Current address: IBM, Boca Raton, FL 33431.

[1] See *Chemical Physics of Intercalation II,* edited by P. Bernier, J. Fischer, S. Roth, and S. Solin, NATO ASI Ser. B, Vol. 305 (Plenum, New York, 1993), p. 283.

[2] M. Winokur, in *The Handbook of Conducting Polymers,* edited by T. Skotheim, R. Elsenbaumer, and J. Reynolds (Mercel-Dekker, New York, 1997), 2nd ed.

[3] M. B. Geilikman, Sov. Phys. JETP **39**, 570 (1974); O. G. Mouritsen and A. J. Belinsky, Phys. Rev. Lett. **48**, 181 (1982); A. B. Harris, O. G. Mouritsen, and A. J. Berlinsky, Can. J. Phys. **62**, 915 (1984).

[4] H.-Y. Choi, A. B. Harris, and E. J. Mele, Phys. Rev. B **40**, 3766 (1989); H.-Y. Choi and E. J. Mele, Phys. Rev. B **40**, 3439 (1989).

[5] A. B. Harris, Phys. Rev. B **50**, 12 441 (1994).

[6] M. J. Winokur *et al.,* Phys. Rev. Lett. **58**, 2329 (1987).

[7] G. Mao, M. J. Winokur, and F. E. Karasz, Phys. Rev. B **53**, R463 (1996).

[8] G. Mao and M. J. Winokur, Synth. Met. **101**, 124 (1999).

[9] D. Chen, M. J. Winokur, M. Masse, and F. E. Karasz, Phys. Rev. B **41**, 6759 (1990).

[10] N. S. Murthy, L. W. Shacklette, and R. H. Baughman, Phys. Rev. B **40**, 12 550 (1989); N. S. Murthy *et al.,* Solid State Commun. **78**, 691 (1991).

[11] R. Elsenbaumer *et al.,* Synth. Met. **11**, 251 (1985).

[12] L. W. Shacklette and J. E. Toth, Phys. Rev. B **32**, 5892 (1985).

[13] T. Granier *et al.,* J. Polym. Sci. Polym. Phys. Ed. **24**, 2793 (1986).

[14] D. Chen, M. J. Winokur, M. A. Masse, and F. E. Karasz, Polymer **33**, 3116 (1992).

[15] J. Barker, D. Baldwin, and D. Bott, Synth. Met. **28**, D127 (1989).

[16] D. Chen, Ph.D. thesis, University of Wisconsin, 1991; G. Mao, Ph.D. thesis, University of Wisconsin, 1997.

[17] Since the intrachannel ion spacing varies, equal proportions of each are not required.

[18] This phase also appears in the EC cell data.